Evaluation of the shape deviation of non rigid parts from optical measurements

François Thiebaut, Cyril Lacroix, Claire Lartigue, Loïc Andolfatto

The International Journal of Advanced Manufacturing Technology manuscript No.
(will be inserted by the editor)

Evaluation of the shape deviation of non rigid parts from optical measurements

François Thiébaut · Cyril Lacroix · Loïc Andolfatto · Claire Lartigue

Received : date / Accepted : date

Résumé This paper deals with an approach to identify geometrical deviations of flexible parts from optical measurements. Each step of the approach defines a specific issue which we try to respond to. The problem of measurement uncertainties is solved using an original filtering method, which permits to only consider a few number of points. These points are registered on a mesh of the CAD model of the constrained geometry. The shape resulting from deflection can be identified through the finite-element simulation of the part's deformation due to its own weight and the measuring set-up. Finally, geometrical deviations are obtained by subtracting geometrical deflections to measured geometrical deviations. The method is illustrated in an experimental test case.

Keywords Measurement · shape deviation · flexible part · optical measurement

1 Introduction

Knowledge of intrinsic part geometry is essential to assembly simulations [1]. Indeed, the geometry of manufactured parts differs from their nominal geometry due to manufacturing process variations. The actual geometry is generally obtained by surface measurements. The objective is to compare measured data with the design model (more generally the CAD model) to determine whether the manufactured surface lies within the tolerance zone. The

François Thiébaut
LURPA, ENS de Cachan, Univ. Paris-Sud, Universit Paris Saclay, F-94235 Cachan, France
Tel. : +33-1 4740 2996
Fax : +33-1 4740 2200
E-mail: thiebaut@lurpa.ens-cachan.fr

Cyril Lacroix
LURPA, ENS de Cachan, Univ. Paris-Sud, Universit Paris Saclay, F-94235 Cachan, France

Loïc Andolfatto
EPFL, École polytechnique fédérale de Lausanne, Laboratory for Hydraulic Machines, avenue de Cour 33 bis, 1007 Lausanne, Switzerland

Claire Lartigue
LURPA, ENS de Cachan, Univ. Paris-Sud, Universit Paris Saclay, F-94235 Cachan, France

alignment of one surface to another is generally carried out by a 3D transformation (rigid transformation). The more common approach to this process is the Iterative Closest Point approach (ICP) [2].

The inspection of flexible parts is not straightforward as gravity loads as well as part fixturing induce part deformations [3][4]. Flexible part shape is generally assessed when components are in assembly configuration. However, the assembly process generates deformations because of the application of forces and restrictions at fixation points.

In this direction, Ascione and Polini [4] propose to assess part geometry using a fixturing equipment designed in order to reproduce the configuration (location and orientation) of the part to be inspected in its use configuration after assembly. The measurement is performed using a contact probe, which involves a displacement which is negligible compared to the part geometry deviations. The fixture's over-constrained configuration can become an active component of the measurement system and plays a central part in the measurement repeatability. This approach is not automated and it is limited, as it requires to reproduce the configuration for each case.

Recent methods use numerical approaches. Classical techniques for flexible part inspection consist in the acquisition of the part surface and the comparison of the measured data to its CAD model, after performing a transformation to align the data against its nominal model. The acquisition is carried out using optical means as contact probes may involve additional deformations (geometry variations) [5]. The transformation is generally a rigid transformation followed by a deformation applied to the mesh of the CAD model. In [6], a displacement field is added in order to consider the deformations induced by the fixturing, the gravity and those due to the manufacturing process. The objective is to find the form deviation due to the manufacturing process only. Then an identification method is proposed to separate the profile deviation from the part deformation that is due to its flexibility. The method seems promising but the application is performed on simulated data only. Radvar-Esfahlan and Tahan propose an inspection process for non rigid part based on simulation using Finite Element Analysis (FEA) [7]. First the part is set-up onto well-known location support points defining a non over-constrained configuration. Then, deformations due to gravity loads are evaluated by using FEA for which fixturing points are used as boundary conditions. Therefore, the real geometrical deviations can be calculated by considering the rigid transformation from the pre-processed CAD model to the scanned data. Some authors used a similar approach (component measurements and FEA analysis) with the aim of predicting over-constrained assemblies but not component shape deviations [8]. In [9], the method does not require the knowledge of all the fixturing points and only considers partial views of the part. Authors focus on the regions where inspection is required, and use the concept of characteristic points that are part of the partial data model. The use of a partial model implies more simplicity for calculations and for the surface acquisition process that does not need to be complete. In this approach, characteristic points found in different partial views, such as fixation points, holes, corners, etc, are matched with the CAD model. Therefore, the method is similar to classical ones but only takes into account an estimation of the missing fixation points. This method is specifically applied to plastic parts. In another interesting approach, a spring-mass model is defined instead of FEM to simulate deformations on a polygonal mesh [10]. Indeed, the polygonal model of the part can be sampled into a set of punctual masses connected to each other by massless springs. The stiffness of the spring associated to the bending is calculated considering the part thickness and the geometry of the triangular faces of the mesh.

The aim of this paper is to obtain the form deviation of flexible components from part measurements independently of the assembly of the configuration of use. The originality is

that the form deviations only due to the manufacturing process are determined relatively to the free-state of the component instead of the CAD model, as is classically the case. For this purpose, the free shape is evaluated from the CAD model by FEA simulations. Then, the component is measured, using optical means because of their main advantages, in a given configuration for which the set-up is well-known. From the measured shape and considering FEA simulations once again, the form deviations can be calculated. Before detailing our approach it is necessary to clearly define what the geometry of a flexible part is.

2 Geometry of a flexible part

The free state of a component is the shape it should have in the state of absence of gravity [11]. Actually, the shape of the component is generally defined in its configuration of use, i.e. when assembled to other components subjected to external loads. This defines the constrained geometry which is the support to the definition of the CAD model, referred to as $\boldsymbol{S}^{\mathrm{T}}_{nom}$. The free shape, referred to as $\boldsymbol{S}^{\mathrm{T}}_{free}$, is defined when both constraints and effect of gravity are not present. In other words, when all the constraints are applied to the theoretical free shape, the geometry of the component is the one defined by the CAD model (figure 1). It is thus possible to define a relationship given in (1) :

$$\boldsymbol{S}^{\mathrm{T}}_{nom} = \boldsymbol{S}^{\mathrm{T}}_{free} + \boldsymbol{E}^{\mathrm{def}}_{nom} \tag{1}$$

Where $\boldsymbol{E}^{\mathrm{def}}_{nom}$ represents the deformation of the shape under gravity and other applied constraints. The deformation can be calculated using a FEA approach.

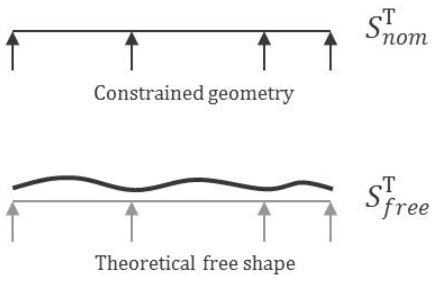

FIGURE 1: Definition of theoretical free shape.

Due to the manufacturing process, the actual shape differs from the theoretical shape, for it includes form deviations.

To obtain form deviations, the component is measured in a measuring configuration which gives the measured shape $\boldsymbol{S}^{meas}_{conf}$. This measured shape includes form deviations but also deformations which are due to the combined effect of the measuring set-up and of the component own weight. These deformations, $\boldsymbol{E}^{def}_{conf}$ can be easily simulated using FEA. Thus, as the free shape is known, it will become simple to identify form deviations. This is detailed in the next section.

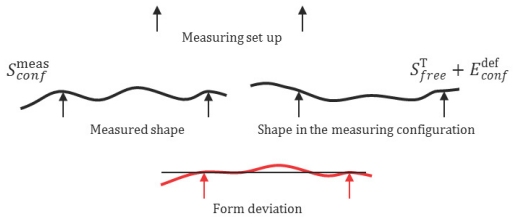

FIGURE 2: Theoretical definition of form deviation.

3 Evaluation of the form deviation

3.1 Principle of the method

The measurement of a flexible component is usually performed in a given configuration, using an over-constrained measuring set-up. In this configuration, the actual shape corresponds to the theoretical free shape, added to the form deviation and the deformation under the combined effect of the measuring set-up and the component's own weight. The treatment of the raw measurement data, detailed in sect. 3.2, yields to the measured shape $\boldsymbol{S}^{\text{meas}}_{conf}$ which can be expressed by eq. (2) :

$$\boldsymbol{S}^{\text{meas}}_{conf} = \boldsymbol{S}^{\text{T}}_{free} + \boldsymbol{E}^{\text{def}}_{conf} + \boldsymbol{E}^{\text{shape}} \tag{2}$$

where $\boldsymbol{E}^{\text{shape}}$ is the form deviation. As stated before, the free shape can easily be deduced from the CAD model using eq. (1) which leads to :

$$\boldsymbol{S}^{\text{T}}_{free} = \boldsymbol{S}^{\text{T}}_{nom} - \boldsymbol{E}^{\text{def}}_{nom} \tag{3}$$

where $\boldsymbol{E}^{\text{def}}_{nom}$ is calculated thanks to FEA simulations. In the same way, $\boldsymbol{E}^{\text{def}}_{conf}$ is evaluated thanks to the simulation of the part deflection under its weight and considering the fixturing of the corresponding measuring configuration. FEA simulations are detailed in subsection 3.4. Finally, the form deviation of the flexible component can be calculated from the measured shape in a configuration using (4) :

$$\boldsymbol{E}^{\text{shape}} = \boldsymbol{S}^{\text{meas}}_{conf} - \boldsymbol{E}^{\text{def}}_{conf} - \boldsymbol{S}^{\text{T}}_{free} \tag{4}$$

The form deviation of a part can be mathematically expressed as a field which is intrinsic to the part and defined in each point of the part surface. Incorporating eq. (3) into eq. (4) yields to :

$$\boldsymbol{E}^{\text{shape}} = \boldsymbol{S}^{\text{meas}}_{conf} - \boldsymbol{E}^{\text{def}}_{conf} - \boldsymbol{S}^{\text{T}}_{nom} + \boldsymbol{E}^{\text{def}}_{nom} \tag{5}$$

So, defining the measured geometrical deviation field, $\boldsymbol{E}^{\text{meas}}$ as $\boldsymbol{E}^{\text{meas}} = \boldsymbol{S}^{\text{meas}}_{conf} - \boldsymbol{S}^{\text{T}}_{nom}$, which represents deviations of the measured shape from the CAD model, the form deviation field is given by :

$$\boldsymbol{E}^{\text{shape}} = \boldsymbol{E}^{\text{meas}} - \boldsymbol{E}^{\text{def}}_{conf} + \boldsymbol{E}^{\text{def}}_{nom} \tag{6}$$

Eq. (6) gives the form deviation of the part expressed in a finite number of points. This corresponds to the geometrical deviation expressed at each node of the mesh which is the support of the FE simulation. The measured geometrical deviation field, $\boldsymbol{E}^{\text{meas}}$, must then be defined at each node of the mesh too as detailed in the next section.

3.2 From measured points to the measured geometrical deviation field

The part is scanned using an optical measuring system to avoid contact, so that the part shape is not impacted during the measurement. As it is interesting to characterize the shape of large parts in short time, a laser plane sensor is chosen to scan the part. The result of the measurement stage is a point cloud, which is dense, non homogeneous and noisy [12]. This point cloud represents the shape of the component in its measuring configuration. As mentioned earlier, the measured geometrical deviation field must be expressed at each node of the mesh. A processing of the raw data is thus necessary to match one node of the mesh to the corresponding point of the point cloud for which the deviation will be calculated. Due to the point density of the scanned data, and considering limit uncertainties associated with optical measuring systems, in particular digitizing noise, it seems relevant to estimate the deviation between the node and its closest neighbors belonging to the point cloud. The use of a vicinity to define the actual geometrical deviation between a measured part and its CAD model has been used in [13]. Authors define the neighborhood by the facets between four points in close correspondence with the considered point, and the geometrical deviation corresponds to the minimum normal distance between the point and each facet. Our approach is quite different as the neighborhood is defined by a cylinder and as we define the geometrical deviation at the considered point by the mean value of all the normal distances. This is performed as follows (see figure 3) :

- Estimation of the normal vector $\mathbf{n_i}$ for each node P_i of the mesh .
- Extraction of the nearest neighbors of the node belonging to the point cloud : the nearest neighbors are the points M_j that belong to a cylinder of radius R (with R = 1 mm in the present work) and whose axis is the normal vector.
- Calculation of the distance $e_{ij} = \overrightarrow{P_iM_j}.\overrightarrow{n_i}$ for each M_j.
- Evaluation of the geometrical deviation $d_i = mean(e_{ij})$ corresponding to the node P_i

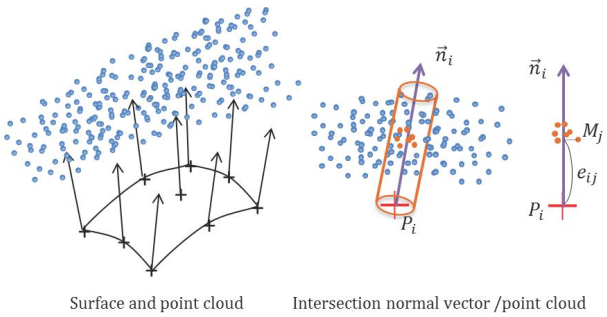

‘

FIGURE 3: Evaluation of the local geometrical deviation

The deviation at each node P_i of the mesh is thus calculated as the mean value of the deviations e_{ij} corresponding to the deviation evaluated along the vector normal between the node and each one of its neighbor. The calculation is only performed if the number of neighbors is greater than a threshold N_t, arbitrarily fixed at $N_t = 10$ in the present work,

that means if the cylinder of radius R whose axis is $\mathbf{n_i}$ contains more than 10 points. During this step, the standard deviation of the deviations is also calculated as follows :

$$\sigma_i = \sqrt{\frac{1}{p-1}\sum_{j=0}^{p}(e_{ij} - d_i)^2)} \tag{7}$$

The evaluation of σ_i gives a cartography of the digitizing noise. The points for which the digitizing noise is high are removed. This leads to areas for which the geometrical deviation d_i cannot be evaluated directly from the measurement. Besides, in some cases, the completeness of the measurement can not be ensured due to accessibility reasons. As a result, the acquired point cloud may present some digitizing holes. In these areas, the direct evaluation of the geometrical deviation is not possible either. Then, for digitizing holes and for highly noisy areas, an extrapolation method of the measured shape is proposed to obtain a complete cartography of the measured geometrical deviations. The approach developed to obtain this complete cartography is summarized in figure 4. First a coarse registration of the rough point cloud to the mesh of the CAD model is manually carried out using the points that define the part set-up. This rough registration allows the alignment of the point cloud to CAD model at about $0.01mm$. Following this step , geometrical deviations d_i are calculated along with local noise (as the standard deviation estimated by eq. (7)). Nodes for which the noise is too high are removed, leading to points for which geometrical deviations are assessed. To obtain the field of measured deviations $\boldsymbol{E}^{\text{meas}}$ at each node of the mesh, a stage of extrapolation based on a modal decomposition is carried out. This step is detailed in the next section.

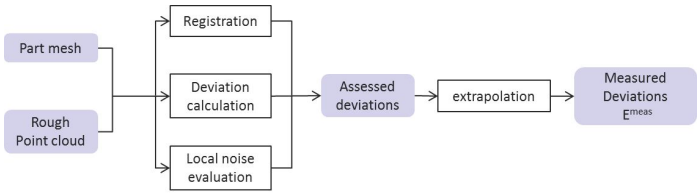

FIGURE 4: From measured points to measured deviations

3.3 Shape deviation expressed as modal coordinates

3.3.1 Modal decomposition

The expression of shape deviation as the discrete field $\boldsymbol{E}^{\text{shape}}$ is not entirely satisfying as it still highly depends on the measurement process definition that leads to a certain amount N of measured points for instance. With no further work to express the measurement result as the intrinsic shape deviation of the part, it is impossible to re-use it for other purposes such as assembly simulation.

Huang and Ceglarek [14] used a decomposition based on direct cosine transform to express the shape deviation of a part. This technique requires to have a structured mesh of the

part. This is not always possible. Franciosa *et al.* [15] proposed to use mesh morphing techniques derived from the computer graphics community to express shape deviation. Although it can describe complex shapes without any assumption on the nominal geometry of the considered parts, the identification of a proper set of morphing operators to fit the evaluated shape deviation can be difficult. Samper and Formosa [16] proposed to express the shape deviation of a part using a modal decomposition based on the part's natural modes. This technique combines both the applicability to whatever part shape and the well-established strategy to identify a finite set of parameters describing the shape deviation. The part's natural modes are given by the solution of the linear dynamic equation :

$$M \cdot \ddot{\boldsymbol{u}} + K \cdot \boldsymbol{u} = 0 \tag{8}$$

with :

— $\boldsymbol{u}$ the displacement of each node for each degree of freedom (DOF) of the meshed part elements ;

— K the stiffness matrix modeling the mechanical behavior of the measured part ;

— M the mass matrix modeling the mass distribution of the measured part.

The solutions of eq. (8) can be written as :

$$\boldsymbol{u}_i(t) = \boldsymbol{q}_i \cdot \cos \omega_i t \tag{9}$$

with ω_i the natural pulsation of the mode i and $\boldsymbol{q}_i$ its amplitude vector.

The number of natural modes that can be computed equals the number of DOFs of the problem, which is $6N_n$ considering the entire finite element model described in subsect. 3.4.

The natural mode amplitude vectors have the property defined in eq. (10) :

$$\boldsymbol{q}_i{}^t \cdot M \cdot \boldsymbol{q}_j = \delta_{ij} \tag{10}$$

with δ_{ij} the Kronecker symbol, equal to 1 if $i = j$ and otherwise zero. Hence the $\boldsymbol{q}_i$ mode amplitude vectors are a basis of the displacement space and the dot product defined in eq. (11) can be used to project any displacement field $\boldsymbol{u}$ on this basis.

$$< \boldsymbol{a}, \boldsymbol{b} >= \boldsymbol{a}^t \cdot M \cdot \boldsymbol{b} \tag{11}$$

As explained in eq. (12) Samper and Formosa use this dot product to identify the modal coordinates $\{\lambda_i\}$ of a particular shape deviation, considering its discrete expression $\boldsymbol{u}$ given for each node of the meshed component.

$$\forall i \in \{1, \ldots, 6N_n\},\ \lambda_i = \boldsymbol{q}_i{}^t \cdot M \cdot \boldsymbol{u} \tag{12}$$

With the ω_i sorted in growing values, the mode amplitude vectors $\boldsymbol{q}_i$ are sorted in increasing complexity. As the wavelength of the mode decreases with the frequency, the entire basis is usually not necessary to depict the shape deviation. A residual noise e_{N_m} kept at the same order of magnitude as the measurement uncertainty provides an efficient criterion to assess the relevance of the selected number N_m of modes of the truncated basis.

$$e_{N_m} = \sqrt{\left(\boldsymbol{u} - \sum_{i=1}^{N_m} \lambda_i \boldsymbol{q}_i\right)^t \cdot \left(\boldsymbol{u} - \sum_{i=1}^{N_m} \lambda_i \boldsymbol{q}_i\right)} \tag{13}$$

Even for complex geometry, around 30 modes provide a difference smaller than $5\,\mu m$ between modal decomposition and actual measurement results [16].

The modal coordinates describing the shape deviation of the part no longer form a discrete description but a parametric one. It can then be used for other purposes such as assembly simulation or best fit. The identification of modal coordinates only requires that the deviation is expressed at each node of the mesh. But this requirement can not always be fulfilled in practice.

3.3.2 Modal decomposition on incomplete set of measurement results

In this paper, the displacement field $\boldsymbol{u}$ is not considered to be known at each node of the meshed used for modal decomposition. Only a subset of its component, written $\tilde{\boldsymbol{u}}$, can be extracted from the shape deviation $\boldsymbol{E}^{\text{shape}}$ obtained according to eq. (4). The same dimension reduction that yields $\tilde{\boldsymbol{u}}$ out of $\boldsymbol{u}$ is applied to provide the reduced mode amplitude vectors $\tilde{\boldsymbol{q}}_i$ out of each $\boldsymbol{q}_i$ and the reduced mass matrix $\tilde{M}$ out of M. Then :

$$\begin{cases} \forall i \in \{1,\dots,N_m\},\ \mu_i = \sqrt{\tilde{\boldsymbol{q}}_i{}^t \cdot \tilde{M} \cdot \tilde{\boldsymbol{q}}_i} \\ \forall (i,j) \in \{1,\dots,N_m\}^2,\ i \neq j,\ \mu_{ij} = \sqrt{\tilde{\boldsymbol{q}}_i{}^t \cdot \tilde{M} \cdot \tilde{\boldsymbol{q}}_j} \end{cases} \tag{14}$$

and :

$$\begin{cases} \forall i \in \{1,\dots,N_m\},\ \tilde{\lambda}_i = \tilde{\boldsymbol{q}}_i{}^t \cdot \tilde{M} \cdot \tilde{\boldsymbol{u}} \\ \forall i \in \{1,\dots,N_m\},\ |\tilde{\lambda}_i - \lambda_i| < \max\limits_{i \in \{1,\dots,N_m\}, j \neq i} |\mu_{ij}| \end{cases} \tag{15}$$

The $\tilde{\lambda}_i$ are the approximated modal coordinates identified with the shape deviation defined on a subset of the mesh nodes. The impact of the dimension reduction on the modal coordinates identification can be assessed by evaluating the maximum value of the μ_{ij}.

Shape deviation expressed only for local areas of the part – due to accessibility issues – is likely to increase the value of the μ_{ij}. It is the consequence of the inability of global techniques such as modal decomposition to express local results.

A comprehensive expression of the shape deviation will provide negligible μ_{ij} and then an accurate evaluation of the modal coordinates. With the shape deviation expressed for all the nodes of the meshed part, the μ_{ij} will equal 0. This particular case is the one for which the strategy proposed in [16] and described in subsubsect. 3.3.1 is applicable.

3.4 Gravity and constraint effect

As mentioned in subsect. 3.1, the deformation $\boldsymbol{E}^{\text{def}}$ is due to both the gravity and to the constraints associated with the configuration (which can be the measuring configuration or the nominal configuration). Considering that the mechanical behavior of the part to be measured is known, it can be predicted thanks to a simulation model. As in many approaches presented in the literature, some of them detailed in [1,7], a finite element simulation model has been found appropriate to predict this behavior.

As the finite element simulation required the part to be meshed, all the discrete deviation fields $\boldsymbol{E}^{\text{shape}}$, and $\boldsymbol{E}^{\text{def}}$ are expressed on a subset of N points corresponding to the nodes of the part mesh.

Meshing almost always involves simplification of the part geometry. This paper addresses the measurement of flexible parts that are usually thin, such as sheet metals parts.

This type of parts can be well-modeled with shell elements, requiring the part to be simplified as a single surface. Even if it can be bypassed, using the simplified measured surface makes the flow quite easier. This particular case is assumed in the following.

With the same notations used in eq. (8), a finite element simulation can be mathematically described as consisting in finding $\boldsymbol{u}$ satisfying the following equations :

$$\begin{cases} K \cdot \boldsymbol{u} = \boldsymbol{f} + M \cdot \boldsymbol{g} \\ C \cdot \boldsymbol{u} = \boldsymbol{d} \end{cases} \tag{16}$$

with :

— $\boldsymbol{g}$ a vector modeling the gravity at each node of the meshed part and along each DOF ;

— $\boldsymbol{f}$ a vector describing the external mechanical actions apart from gravity, such as clamping forces ;

— C and $\boldsymbol{d}$ a matrix and a vector modeling the kinematic boundary conditions, such as an imposed displacement due to known contact on the measurement set-up.

Classically, the small perturbations hypothesis is adopted. The displacement of each point is assumed to be small, and the gradient of deformations can be neglected before the unit. As an obvious result, actual stiffness and nominal stiffness can be merged. Therefore, loading can be applied on the nominal mesh as well as on the deformed mesh. Considering the meshed part has N_n nodes with 6 DOF each [1], the solution $\boldsymbol{u}$ of the finite element problem has $6N_n$ components.

The value of the deformation $\boldsymbol{E}^{\text{def}}$, giving the part deflection for N of the N_n nodes of the part can be directly derived from $\boldsymbol{u}$ by extracting the displacements of the N nodes for which deviations are assessed. First, the approach is used to obtain $\boldsymbol{E}^{\text{def}}_{nom}$, the deformation corresponding to the nominal configuration. Once $\boldsymbol{E}^{\text{def}}_{nom}$ is known, another simulation is performed to obtain $\boldsymbol{E}^{\text{def}}_{conf}$, the deformation associated with the measuring configuration. Finally, the discrete shape deviation field $\boldsymbol{E}^{\text{shape}}$ is obtained by subtracting the deformations to the measured deviation $\boldsymbol{E}^{\text{meas}}$ as proposed in eq. (6).

4 Experimental validation

In order to illustrate the proposed method, a sheet metal part in aluminum alloy is measured. The CAD model of the part is a cylinder surface of radius R = 1m set in an over-constrained configuration defined by 4 contact pads. First, a simulation is necessary to obtain $\boldsymbol{E}^{\text{def}}_{nom}$.

For this purpose, the part is meshed, and the simulation is performed considering that normal displacements are not allowed at the 4 contact points, and that the part is under the effect of gravity. Finite Element simulations are conducted using CATIA V5 ©, considering 2D shell elements. The simulation yields $\boldsymbol{E}^{\text{def}}_{nom}$. $\boldsymbol{S}^{\text{T}}_{free}$ is thus obtained using equation (3) (see figure 6).

Next, the part is set in different equally-constrained configurations considering only 3 contact pads, as displayed in figure 5. The use of more than one configuration will highlight the method ability to evaluate the intrinsic shape deviation of the part independently from the measurement setup. The configuration is easily modified by changing the locations of these contact pads. As the part is flexible, the part is scanned using a laser-plane sensor

1. 3 translations and 3 rotations.

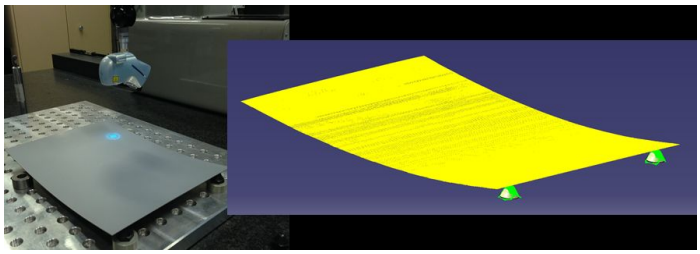

FIGURE 5: Part measurement.

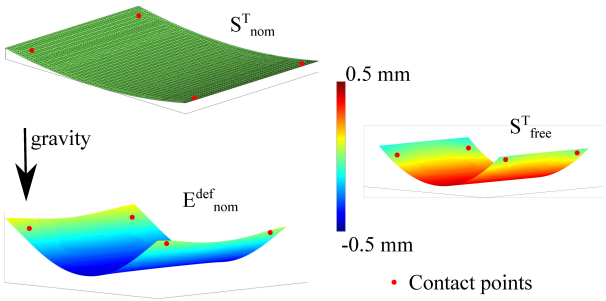

FIGURE 6: Calculation of $\boldsymbol{S}^{\mathrm{T}}_{free}$

mounted on a CMM whose geometrical errors are negligible (about 4 μm in the working space). The sensor orientation is kept constant during the whole measurement step. As only one sensor orientation is used, there is no additional error due to sensor repositioning. The sensor accuracy is assessed via a protocol. The trueness is evaluated to 10 μm for a gauge of 35 mm, which is consistent with the order of magnitude of the expected deformations [18].

Once the part is measured, the following step is the calculation of the measured deviation field, $\boldsymbol{E}^{\mathrm{meas}}$ as detailed in subsection 3.2. For each node of the CAD mesh, the deviation d_i is calculated along with the standard deviation σ_i given by equation (7). As proposed in our approach (see figure 4), data are pre-processed and filtered by removing points for which the digitizing noise ($\delta_i = k.\sigma_i$, with k = 1) is greater than the mean noise associated with the sensor. The mean noise of the sensor is generally evaluated thanks to a protocol and according to the digitizing distance and the digitizing angle [12] [17]. For the used measuring conditions, the mean noise associated to the sensor is equal to δ_{sensor} = 0.02 mm. As a result, points for which $\delta_i > 0.03$ mm are tagged as too noisy. For such points, the geometrical deviation cannot be directly calculated and the measured deviation field is thus extrapolated at the corresponding nodes thanks to the method detailed in subsection 3.3. This is illustrated for first measurement configuration in figure 7. Considering the cartography of the local noise (figure 7-a), deviations are only calculated for nodes such as $\delta_i < 0.03$ mm. This yields to an incomplete cartography of measured deviations ((figure 7-b). Following, the field of measured deviations is reconstructed using the modal decomposition (figure 7-c).

The next step is Finite Element simulations, considering the measurement configuration to obtain $\boldsymbol{E}^{\mathrm{def}}_{conf}$. The normal displacements are not allowed at the 3 contact points defining the measurement set-up (boundary conditions), and once more, the external force is

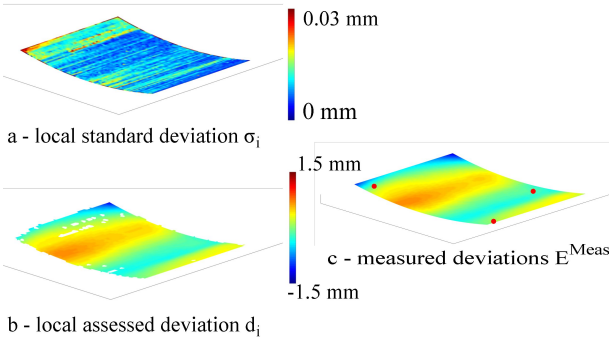

FIGURE 7: Evaluation of the measured deviation field, $\boldsymbol{E}^{meas}$

only gravity. Finally, the field of shape deviation is calculated using equation (6). This is illustrated in figure 8 for configuration 1.

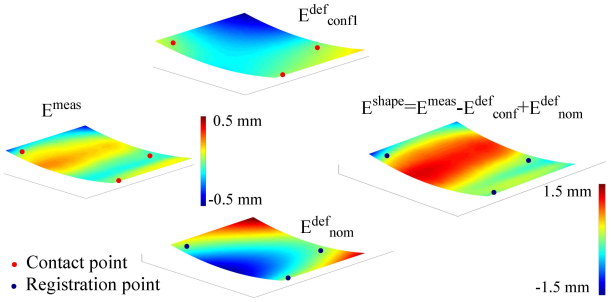

FIGURE 8: Evaluation of the shape deviation field

The whole approach is applied to the second configuration. The measurement set-up is modified by moving the positions of 2 of the 3 contact pads. Only the final result is reported in figure 9. To compare both fields, the result for the second configuration is registered on the contact points of the first configuration. The figure clearly highlights that the field of shape deviations is quite identical for both configurations. In particular, the cartography of the difference between the fields obtained with the two configurations shows that the difference is less than 0.02 mm for most of the part. The difference reaches up to 0.06 mm at the left corner. This is likely due to deviation field reconstruction in this area (see figure 7-b)). Reconstruction is less efficient in areas where the lack of points is significant.

5 Conclusion

An efficient approach to evaluate shape deviations of flexible parts has been proposed in the paper. The method relies on part measurements coupled with FE simulations in order to take into account the deformation associated with gravity and with the measurement

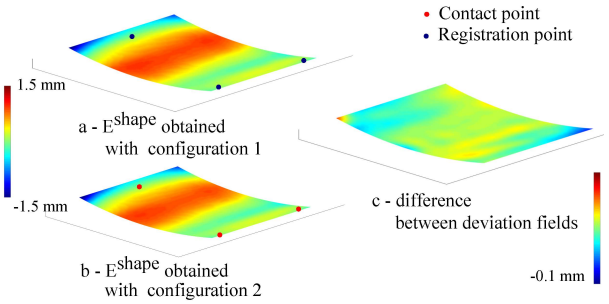

FIGURE 9: Difference between deviation fields considering 2 measurement configurations

configuration. Applied to a simple part for which the mechanical model is well-known, the method allows the identification of the form deviations whatever the measurement configuration. Differences between the deviation fields obtained from 2 different configurations, around a few micrometers, lay within the measurement uncertainty which shows that the method is promising. Future works will focus on more complex parts. In this case, FE simulations require the simplification of the geometrical model and an a priori model registration to simplify calculations. Finally, the approach proves to be an interesting tool to obtain the component's geometry of an assembly in its use configuration, thus eliminating the use of jigs, generally very expensive.

Références

1. P. Breteau *Simulation d'assemblage flexible par la mesure - Application au domaine de l'aéronautique* PhD these, (2009), Ecole Normale Supérieure de Cachan
2. Y. Li, P. Gu *Inspection of free-form shaped parts* Robotics and Computer-Integrated Manufacturing, 21(45),(2005), 421-430
3. G.N. Abenhaim, A. Desrochers, A.S. Tahan *An Investigation of the Repeatability of Nonrigid Parts Measurements : A Case Study of an Aluminum Panel* Procedia, 10, (2013), 105-111
4. R. Ascione, W. Polini *Measurement of nonrigid freeform surfaces by Coordinate Measuring Machine* International Journal of Advanced Manufacturing Technology, 51, (2010), 1055-1067
5. A. Weckenmann, M. Knauer, T. Killmaier *Uncertainty of coordinate measurements on sheet-metal parts in the automotive industry* Journal of Materials Processing Technology, 115(1), (2001), 9-13
6. G. N. Abenhaim, A. S.Tahan, A. Desrochers, R. Maranzana *A novel approach for the inspection of flexible parts without the use of special fixtures* Journal of Manufacturing Science and Engineering, 133, (2011), 1-11
7. H. Radvar-Esfahlan, S-A. Tahan *Nonrigid geometric metrology using generalized numerical inspection fixtures* Precision Engineering, 36(1), (2012), 1-9
8. I. Gentilini, K. Shimada *Predicting and evaluated the post-assembly shape of thin-walled components via 3D laser digitization and FEA simulation of the assembly process* Computer-Aided Design, (43), (2011), 316-328
9. A. Jaramillo, F. Prieto, P. Boulanger *Fast dimensional inspection of deformable parts from partial views* Computers in Industry, 64(9), (2013), 1076-1081
10. A. Jaramillo, F. Prieto, P. Boulanger *Deformable part inspection using a springmass system* Computer-Aided Design, 45(89), (2013), 1128 - 1137
11. C. Lartigue, F. Thiébaut, P. Bourdet, N. Anwer *Dimensional metrology of flexible parts : Identification of geometrical deviations from optical measurements* Series on Advances in Mathematics for Applied Sciences, 72, (200-), 196-203

12. C. Lartigue, A. Contri, P. Bourdet *Digitised point quality in relation with point exploitation* Measurement, 32, (2002), 193-203
13. S. Ravishankar, H. N. V. Dutt, B. Gurumoorthy *AIWINa fast and jigless inspection technique for machined parts* The International Journal of Advanced Manufacturing Technoly, 62, (2012) 231240
14. W. Huang, D. Ceglarek *Mode-based Decomposition of Part Form Error by Discrete-Cosine-Transform with Implementation to Assembly and Stamping System with Compliant Parts* CIRP Annals - Manufacturing Technology, 51(1), (2002), 21-26
15. P. Franciosa, S. Gerbino, S. Patalano, *Simulation of variational compliant assemblies with shape errors based on morphing mesh approach* The International Journal of Advanced Manufacturing Technology, (2010), 1-15
16. S. Samper, F. Formosa *Form Defects Tolerancing by Natural Modes Analysis*, Journal of Computing and Information Science in Engineering, 7(1), (2007), 44-51
17. N. Audfray, C. Mehdi-Souzani, C. Lartigue *Assistance to automatic digitizing system selection for 3D part inspection* ASME 2012 11th Biennial Conference on Engineering Systems Design And Analysis, ESDA2012, Nantes (France), CDRom paper N 82319, (2012)
18. C. Mehdi-Souzani, Y. Quinsat, C. Lartigue, P. Bourdet *A knowledge database of qualified digitizing systems for the selection of the best system according to the application* CIRP Journal of Manufacturing Science and Technology, 13, (2016), 15-23